SAND2015-9289C

Exceptional service in the national interest

Sandia National Laboratories

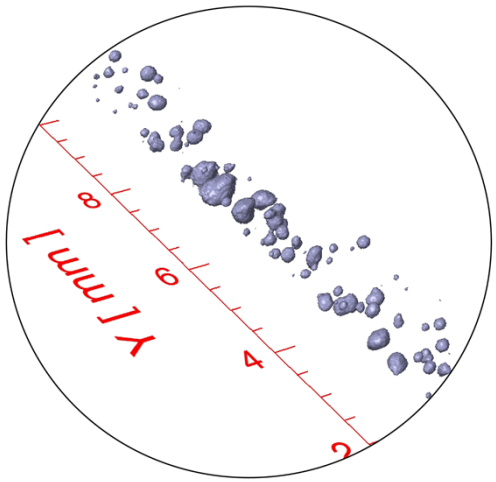

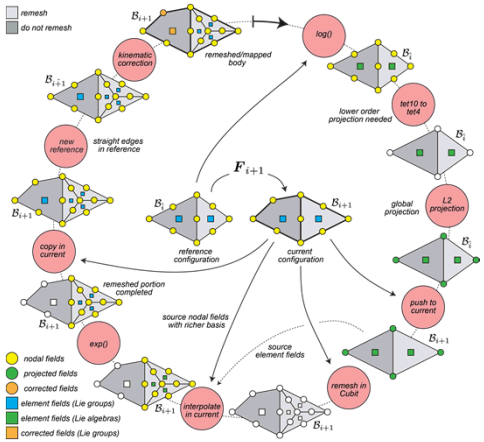

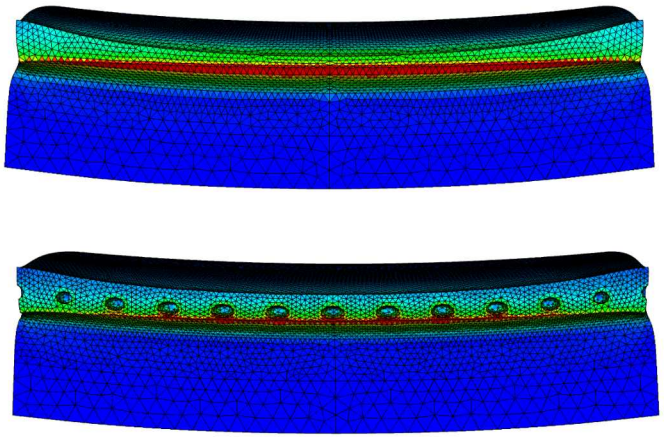

Resolving the evolution of pore structures in 304-L laser welds

J. Foulk, M. Veilleux, J. Emery, J. Madison, H. Jin, J. Ostien, A. Mota

USNCCM 13, San Diego, July 30, 2015

U.S. DEPARTMENT OF ENERGY

National Nuclear Security Administration

Sandia National Laboratories is a multi-program laboratory managed and operated by Sandia Corporation, a wholly owned subsidiary of Lockheed Martin Corporation, for the U.S. Department of Energy's National Nuclear Security Administration under contract DE-AC04-94AL85000. SAND NO. 2011-XXXXP

Foundational engineering problem – laser welds

Surface observations indicate that the failure of 304-L is a primarily a necking process. Interrupted testing will determine the role of crack initiation.

Hypothesis: Pore size and distribution can aid the necking process and crack initiation

- μ-CT needed to probe initial and interrupted pore structures
- Remeshing/mapping needed to resolve the evolution of pore structure
- Homogenization not applicable

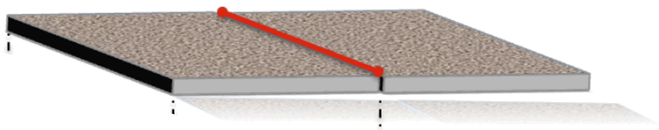

304-L butt weld

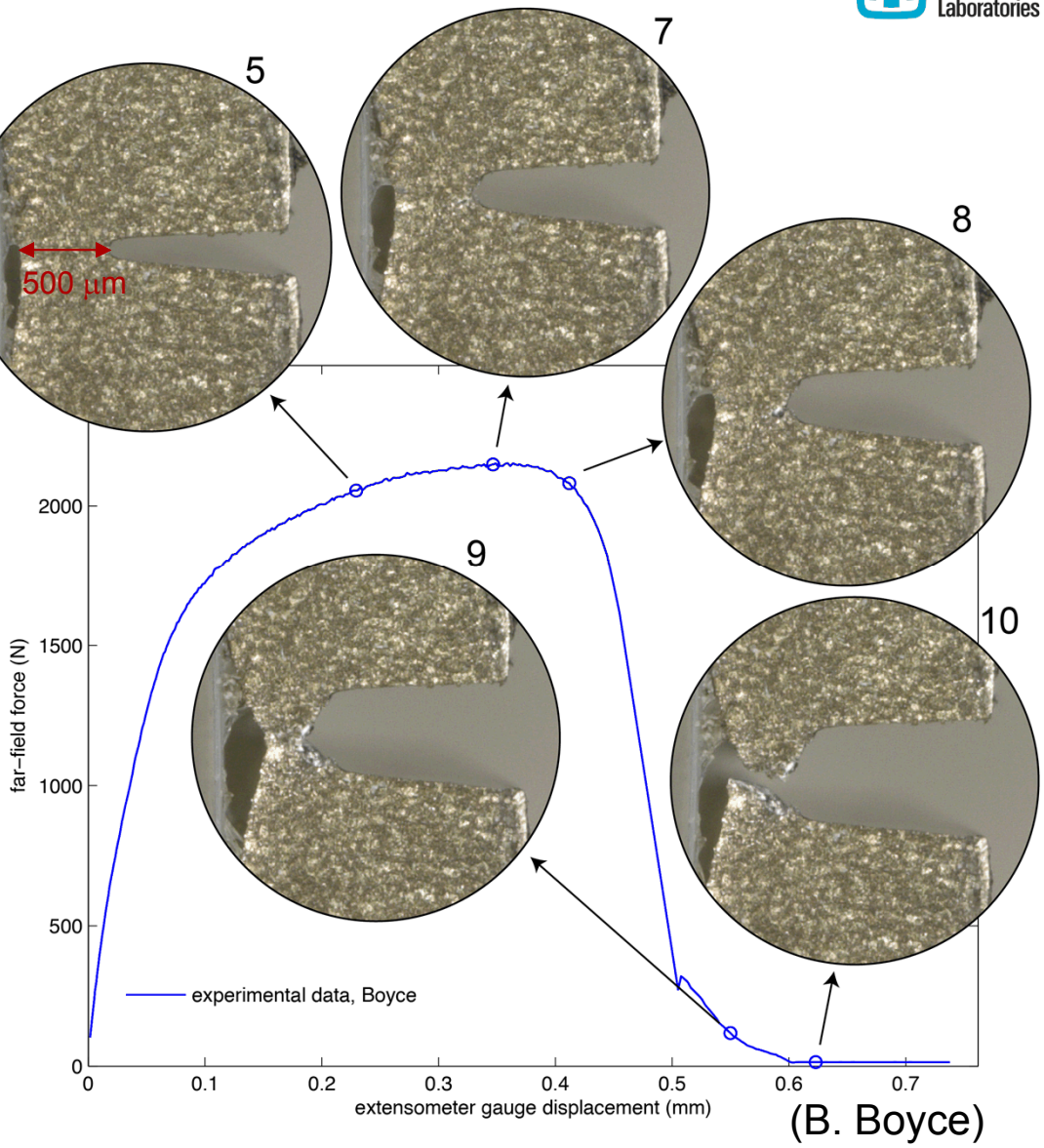

(B. Boyce)

Pores large relative to the ligament – homogenization n/a

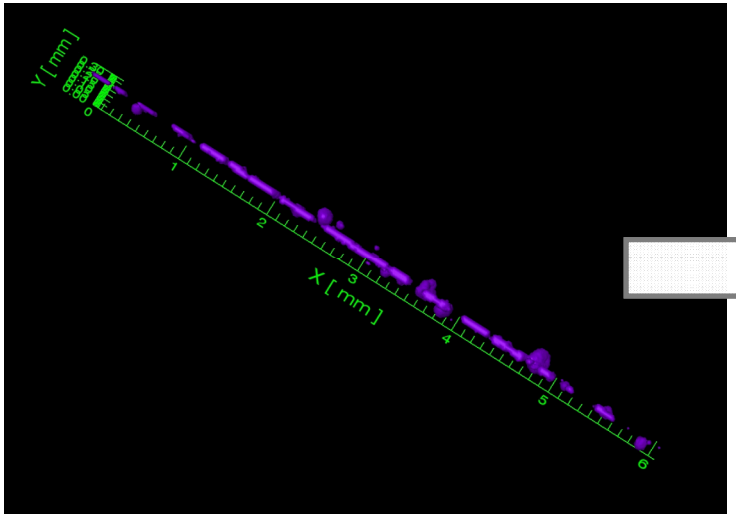

μ-Computed Tomography

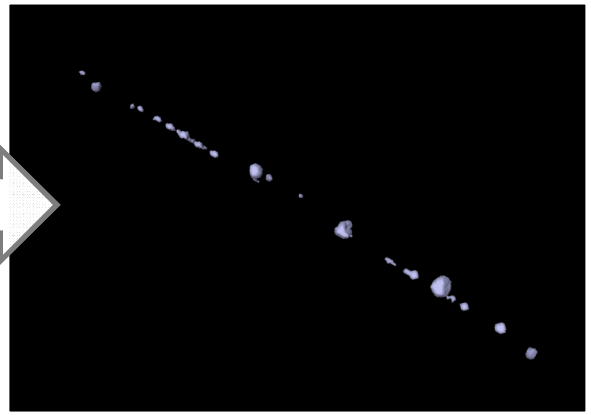

Magnification: 9X
Voxel size: 14 μm
Energy: 130 keV

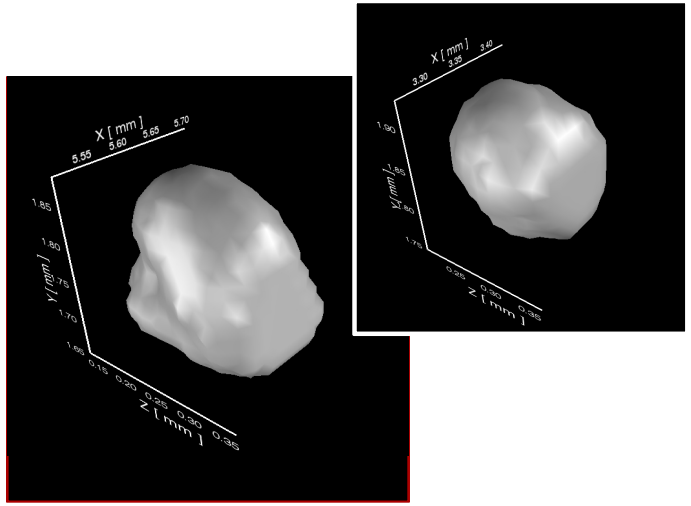

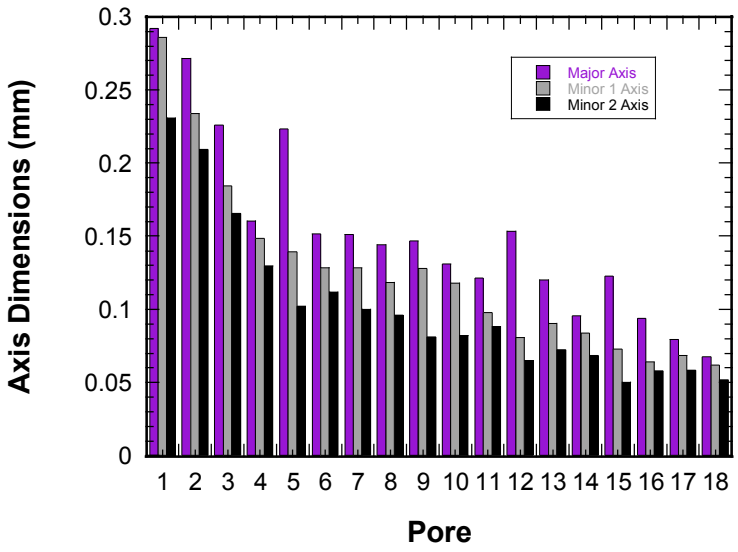

J. Madison, L. K. Aagesen, *"Quantitative Characterization of Porosity in Laser Welds of Stainless Steel"* SCRIPTA MATERIALIA (2012)

Do the pores dominant the deformation process?

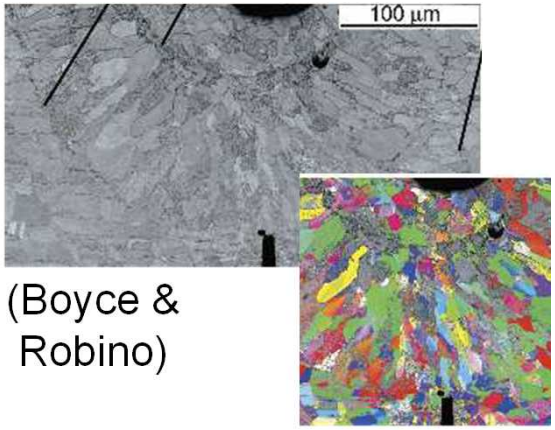

(Boyce & Robino)

What elements of microstructure dominate the load-bearing capacity?

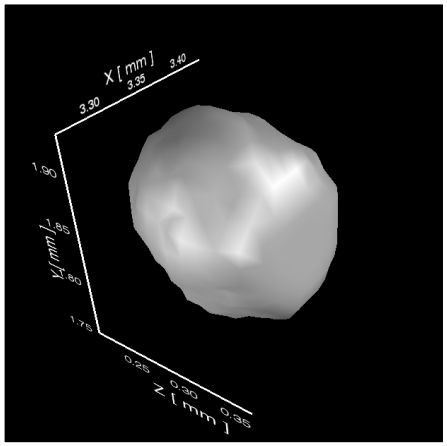

(Madison)

- We hypothesize that pores are the dominant microstructural feature
- We adopt J_2 plasticity for both the base material and the weld
- We have lumped dislocation structures, deformation twinning, and martensitic phase transformations into a phenomenological model for hardening and recovery

sheet thickness: 1.6 mm
ligament length: 508 μm
pore diameter: 150 μm
area fraction: 0.066

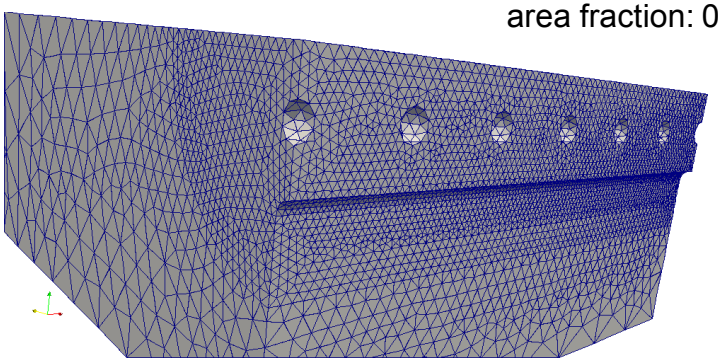

NOTE: Unlike experiments, simulation can systematically increase complexity. Pores first.

Initial efforts w/pores problematic – remeshing needed

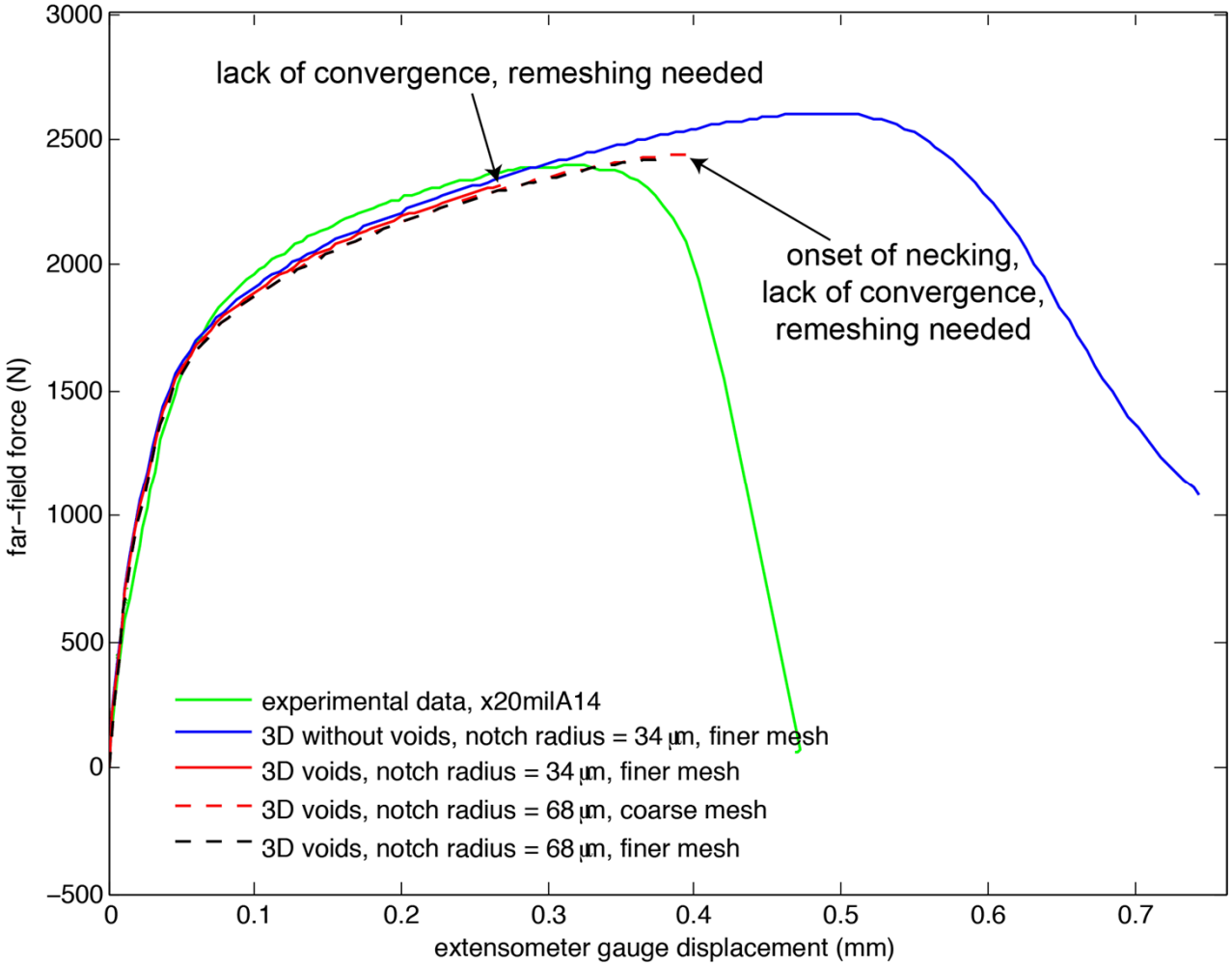

notch radius: 68 μm

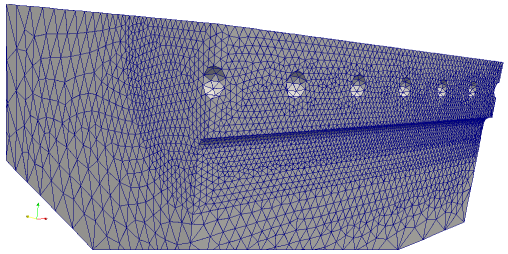

Onset of necking
notch radius = 68 μm
coarse mesh

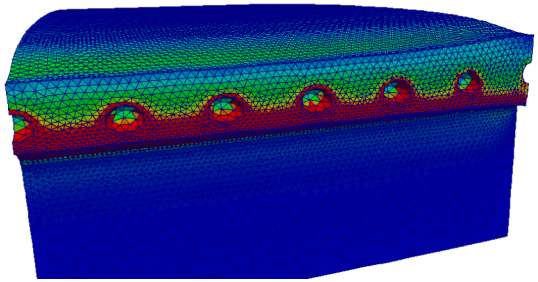

NOTE: Same constitutive model employed for cases with and without voids

Deeper-penetration welds provide additional motivation

Weld schedule impacts porosity. Porosity impacts performance.

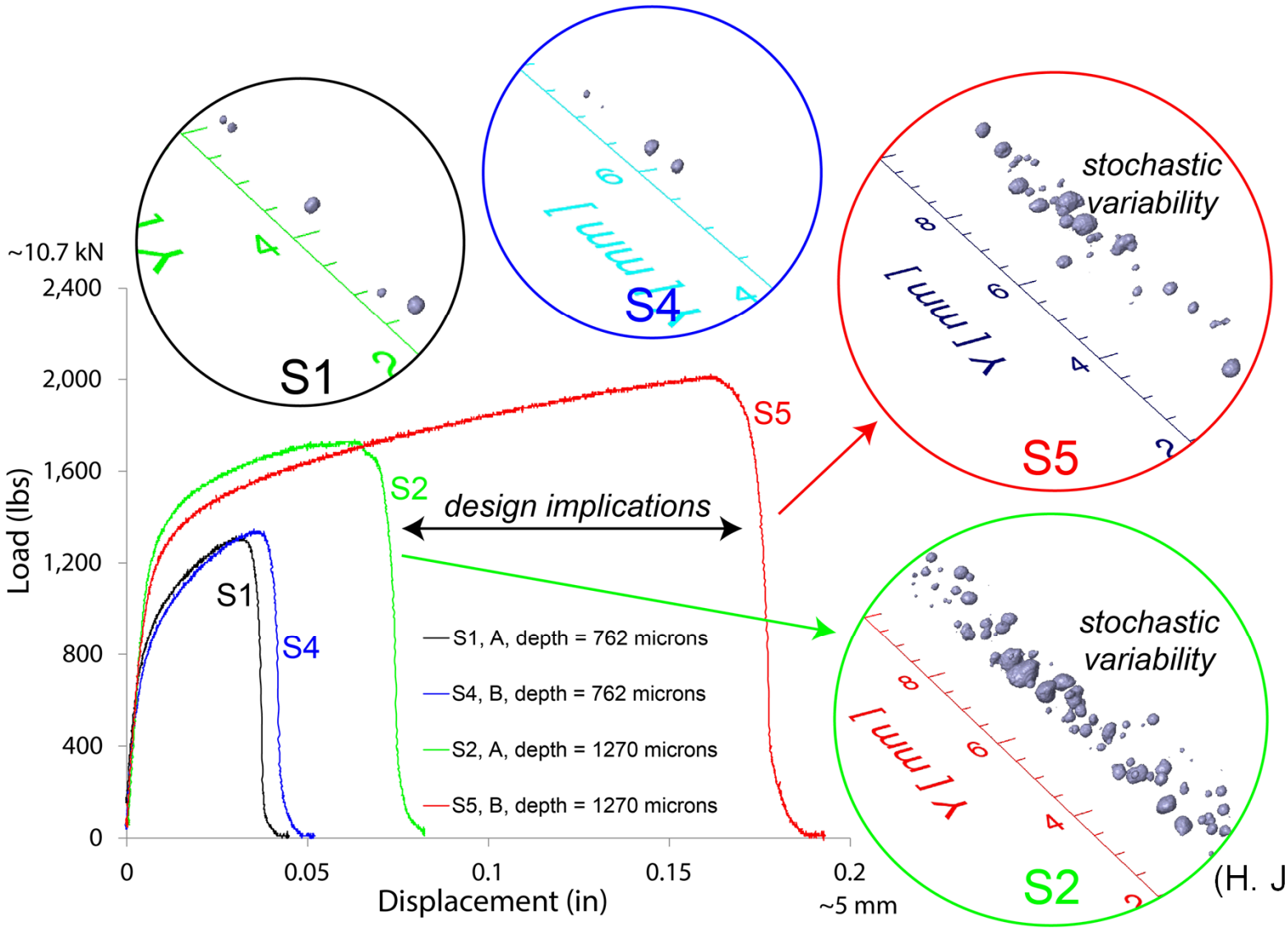

(H. Jin, J. Madison)

Pore size/distribution varies with weld schedule

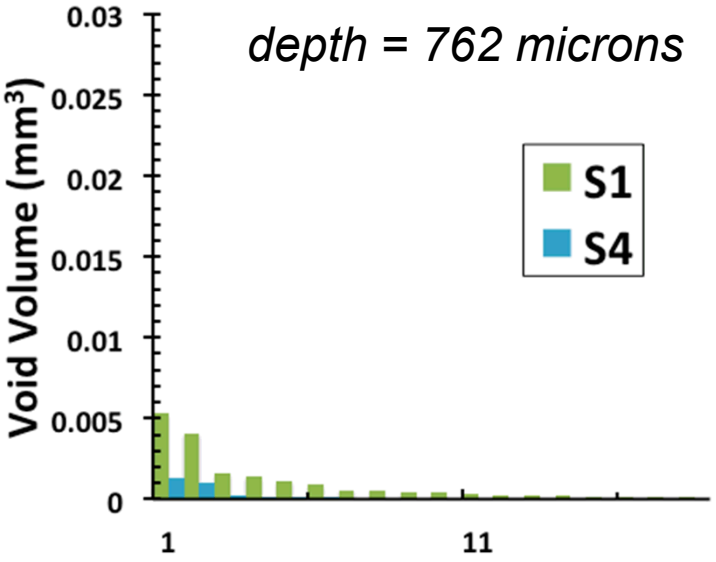

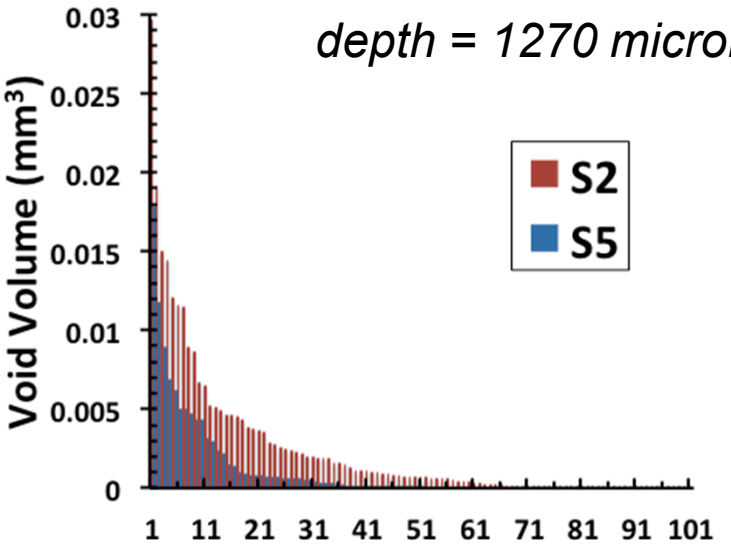

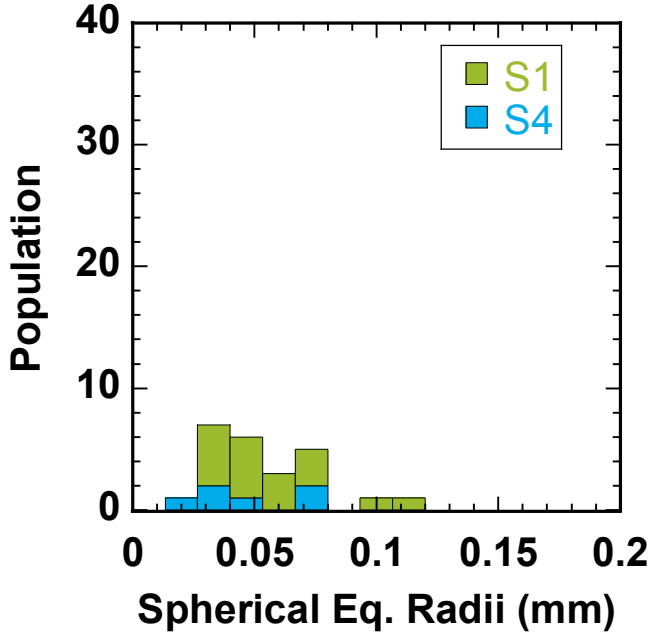

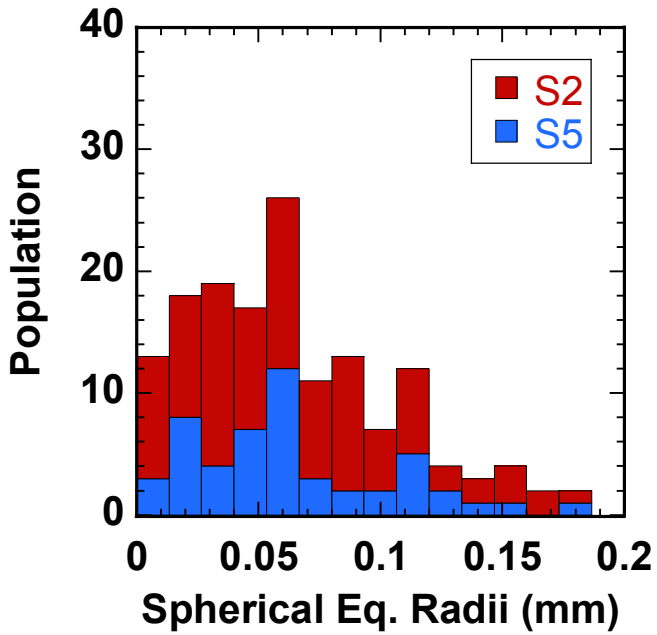

Our approach: mapLL (L_2 + Lie Group/Algebra)

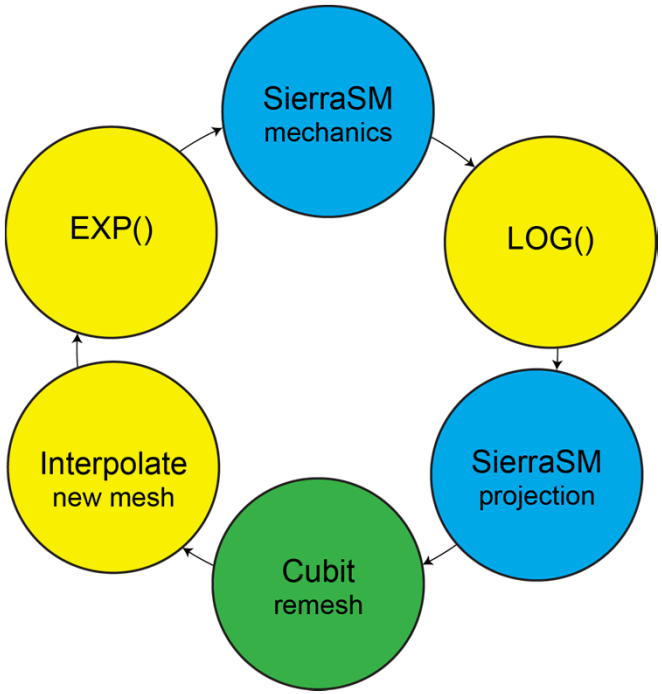

$$\Phi[\boldsymbol{\varphi}, \bar{\boldsymbol{z}}, \bar{\boldsymbol{y}}] := \int_B W(\boldsymbol{F}, \bar{\boldsymbol{z}})\, dV + \int_B \bar{\boldsymbol{y}} \cdot (\bar{\boldsymbol{z}} - \boldsymbol{z})\, dV - \int_B \rho_0 \boldsymbol{B} \cdot \boldsymbol{\varphi}\, dV - \int_{\partial_T B} \boldsymbol{T} \cdot \boldsymbol{\varphi}\, dS$$

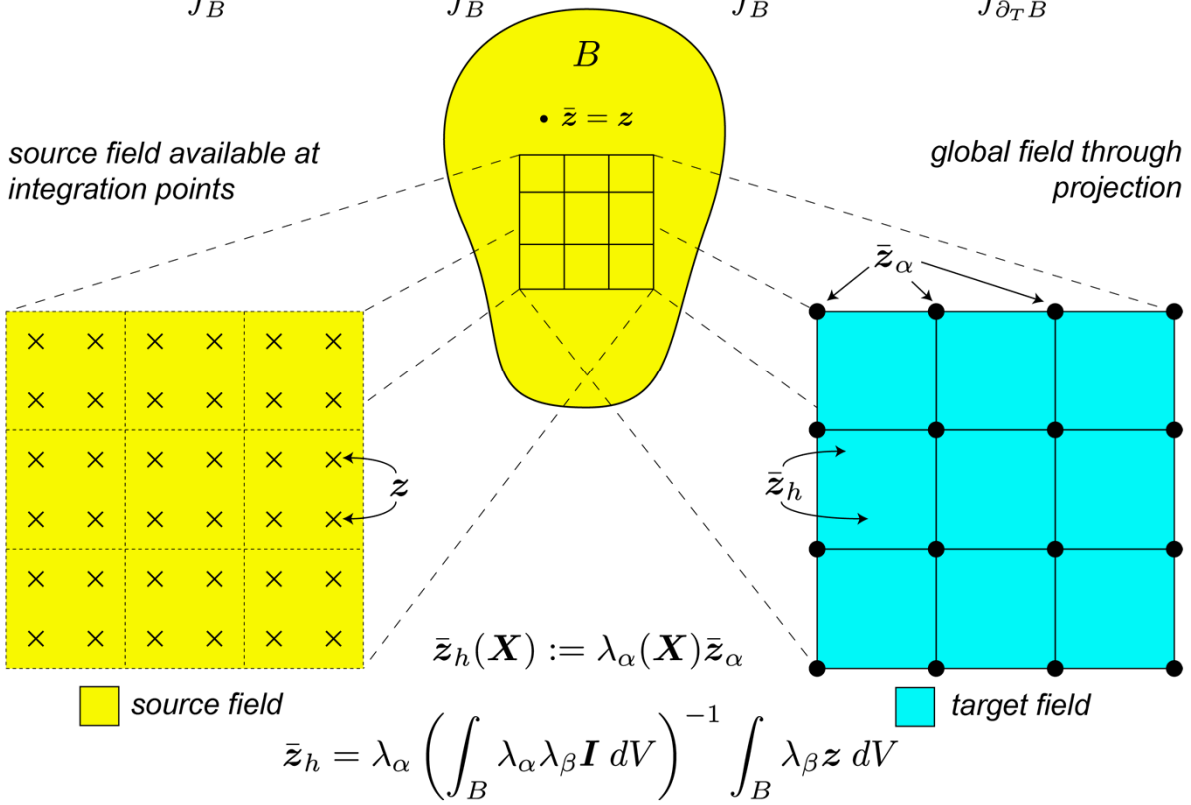

- The variational principle naturally yields an optimal, L_2 projection
- The spaces of variables (Lie algrebra, Lie Group) are honored through log() and exp()
- Advocated by Mota, et. al., Computational Mechanics, 2013

  Past works: Ortiz and Quigley (1991), Radovitzky and Ortiz (1999), Rashid (2002), Jiao and Heath (2004)

New tetrahedral element technology – gradient operator

Sandia National Laboratories

Motivated by prior work of Thoutireddy, et. al., IJNME (2002)

$$\bar{\boldsymbol{F}}(\boldsymbol{X}) := \bar{\boldsymbol{\mathcal{B}}}_a(\boldsymbol{X})\boldsymbol{x}_a$$

$$\bar{\boldsymbol{\mathcal{B}}}_a(\boldsymbol{X}) := \lambda_\alpha(\boldsymbol{X})\left[\int_\Omega \delta_{ik}\lambda_\alpha(\boldsymbol{X})\lambda_\beta(\boldsymbol{X})\,\mathrm{d}V\right]^{-1}\int_\Omega \lambda_\beta(\boldsymbol{X})\frac{\partial N_a(\boldsymbol{X})}{\partial X_J}\,\mathrm{d}V\,\boldsymbol{e}_i\otimes\boldsymbol{E}_J\otimes\boldsymbol{e}_k$$

$$\bar{\boldsymbol{\mathcal{B}}}_a(\boldsymbol{\xi}) = \lambda_\alpha(\boldsymbol{\xi})\left[\int_{\Omega_{\boldsymbol{\xi}}} \delta_{ik}\lambda_\alpha(\boldsymbol{\xi})\lambda_\beta(\boldsymbol{\xi})\,\mathrm{d}V_{\boldsymbol{\xi}}\right]^{-1}\int_{\Omega_{\boldsymbol{\xi}}} \lambda_\beta(\boldsymbol{\xi})\frac{\partial N_a(\boldsymbol{\xi})}{\partial \boldsymbol{\xi}}\,\mathrm{d}V_{\boldsymbol{\xi}}\left(\frac{\partial \boldsymbol{\xi}}{\partial X_J}\right)\boldsymbol{e}_i\otimes\boldsymbol{E}_J\otimes\boldsymbol{e}_k$$

$$\bar{\boldsymbol{\mathcal{B}}}_a(\boldsymbol{\xi}) = \bar{\mathcal{L}}_{a;ilk}(\boldsymbol{\xi})\left(\frac{\partial \xi_l}{\partial X_J}\right)\boldsymbol{e}_i\otimes\boldsymbol{E}_J\otimes\boldsymbol{e}_k$$

$$\bar{\boldsymbol{\mathcal{L}}}_a(\boldsymbol{\xi}) = \lambda_\alpha(\boldsymbol{\xi})\delta_{ik}(M_{\alpha\beta})^{-1}\sum_{S=0}^{11}\frac{\partial N_a}{\partial \xi_l}\int_{E_S}\lambda_\beta(\boldsymbol{\xi})\,\mathrm{d}V_{\boldsymbol{\xi}}\,\boldsymbol{e}_i\otimes\boldsymbol{a}_l\otimes\boldsymbol{e}_k$$

$$\bar{\boldsymbol{\mathcal{B}}}_a(\boldsymbol{\xi}) = \bar{\mathcal{L}}_{a;ilk}(\boldsymbol{\xi})\left[\bar{\mathcal{L}}_{b;JlM}(\boldsymbol{\xi})X_{b;M}\right]^{-1}\boldsymbol{e}_i\otimes\boldsymbol{E}_J\otimes\boldsymbol{e}_k$$

$$\bar{B}_{aJ}(\boldsymbol{\xi}) = \bar{L}_{al}(\boldsymbol{\xi})\left[X_{Jb}\bar{L}_{bl}(\boldsymbol{\xi})\right]^{-1}$$

$$\bar{F}_{iJ}(\boldsymbol{\xi}) = x_{ia}\bar{B}_{aJ}(\boldsymbol{\xi})$$

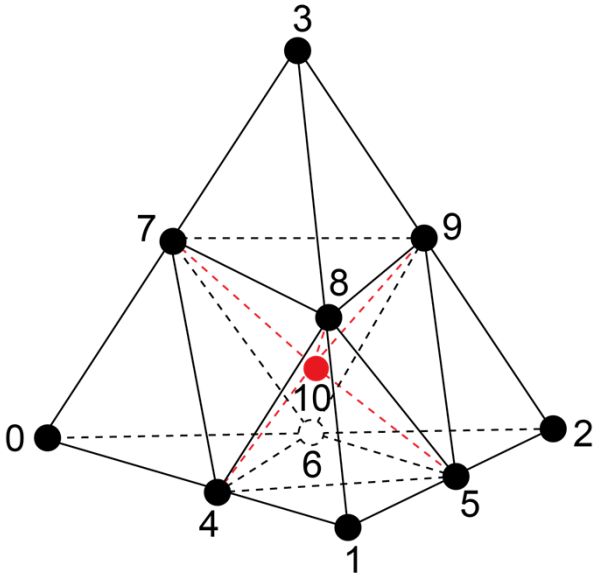

$$\bar{L}_{al}(\boldsymbol{\xi}) \equiv \bar{L}_{10\times 3} = \frac{1}{24}\begin{pmatrix}
9-60\xi_0 & 9-60\xi_0 & 9-60\xi_0 \\
-9+60\xi_1 & 0 & 0 \\
0 & -9+60\xi_2 & 0 \\
0 & 0 & -9+60\xi_3 \\
70(\xi_0-\xi_1) & 2(-4-35\xi_1+5\xi_2+10\xi_3) & 2(-4-35\xi_1+10\xi_2+5\xi_3) \\
2(-1+5\xi_1+40\xi_2-5\xi_3) & 2(-1+40\xi_1+5\xi_2-5\xi_3) & 10(\xi_0-\xi_3) \\
2(-4+5\xi_1-35\xi_2+10\xi_3) & 70(\xi_0-\xi_2) & 2(-4+10\xi_1-35\xi_2+5\xi_3) \\
2(-4+5\xi_1+10\xi_2-35\xi_3) & 2(-4+10\xi_1+5\xi_2-35\xi_3) & 70(\xi_0-\xi_3) \\
2(-1+5\xi_1-5\xi_2+40\xi_3) & 10(\xi_0-\xi_2) & 2(-1+40\xi_1-5\xi_2+5\xi_3) \\
10(\xi_0-\xi_1) & 2(-1-5\xi_1+5\xi_2+40\xi_3) & 2(-1-5\xi_1+40\xi_2+5\xi_3)
\end{pmatrix}.$$

This is exact. Evaluate for your integration scheme.

Volume-averaged formulation does not lock

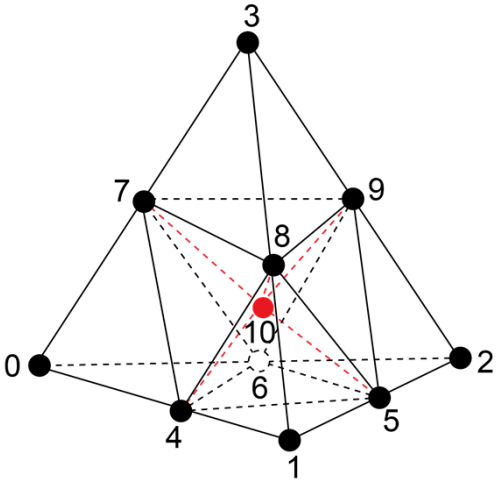

Volume-averaged formulation does not exhibit spurious pressure oscillations.

$$\bar{\boldsymbol{F}}^{\star}(\boldsymbol{\xi}) := \left(\frac{\bar{J}^{\star}}{\bar{J}(\boldsymbol{\xi})}\right)^{\frac{1}{3}} \bar{\boldsymbol{F}}(\boldsymbol{\xi})$$

$$\bar{J}^{\star} := \frac{\int_{\Omega} \bar{J}\,\mathrm{d}V}{\int_{\Omega}\mathrm{d}V}$$

$$\bar{p}^{\star} := \frac{1}{V_{\Omega}} \int_{\Omega} \mathrm{tr}\,\frac{\partial A(\boldsymbol{F}^{\star})}{\partial \bar{\boldsymbol{b}}^{\star}}\,\mathrm{d}V$$

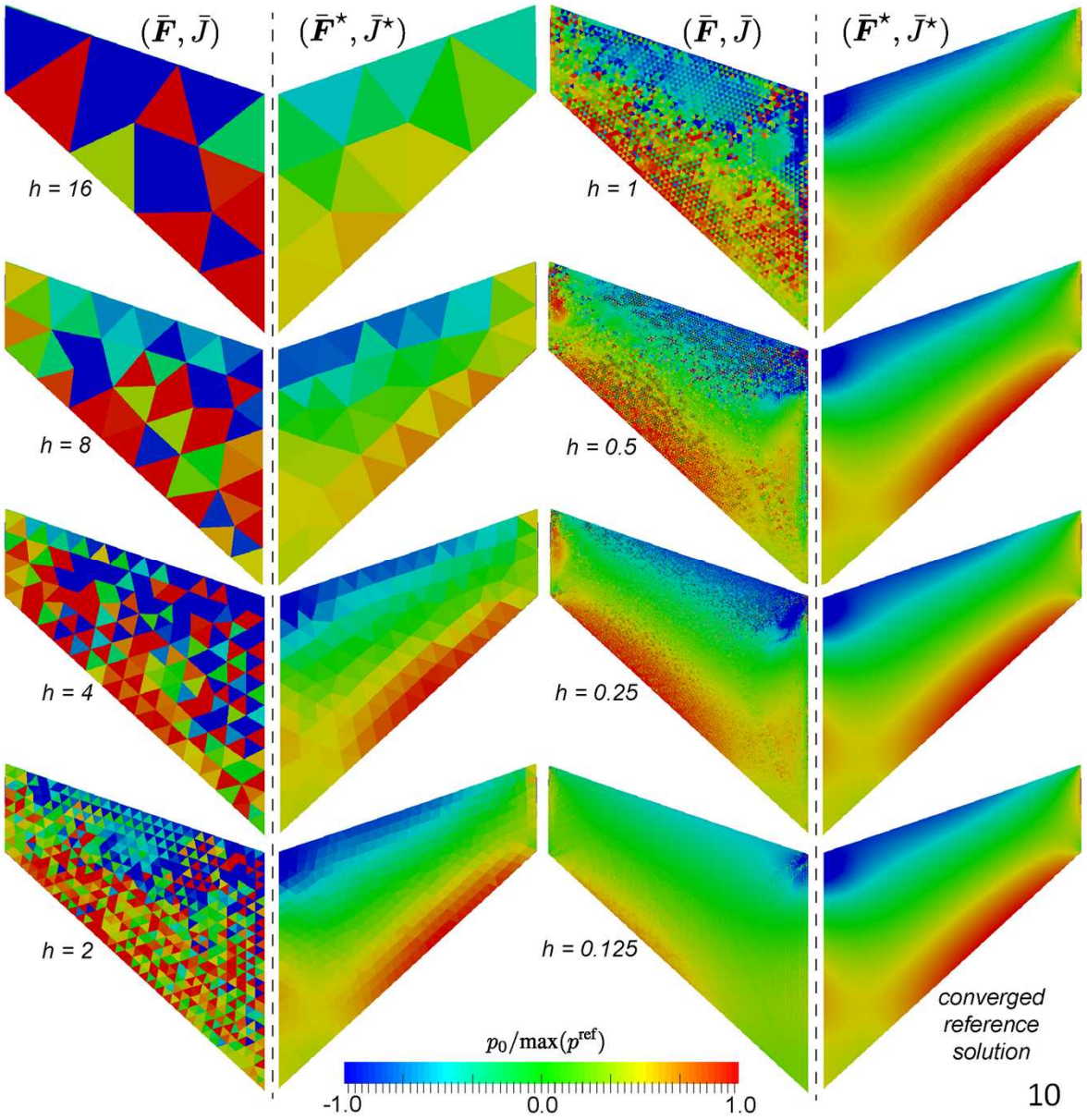

Accommodating local remeshing

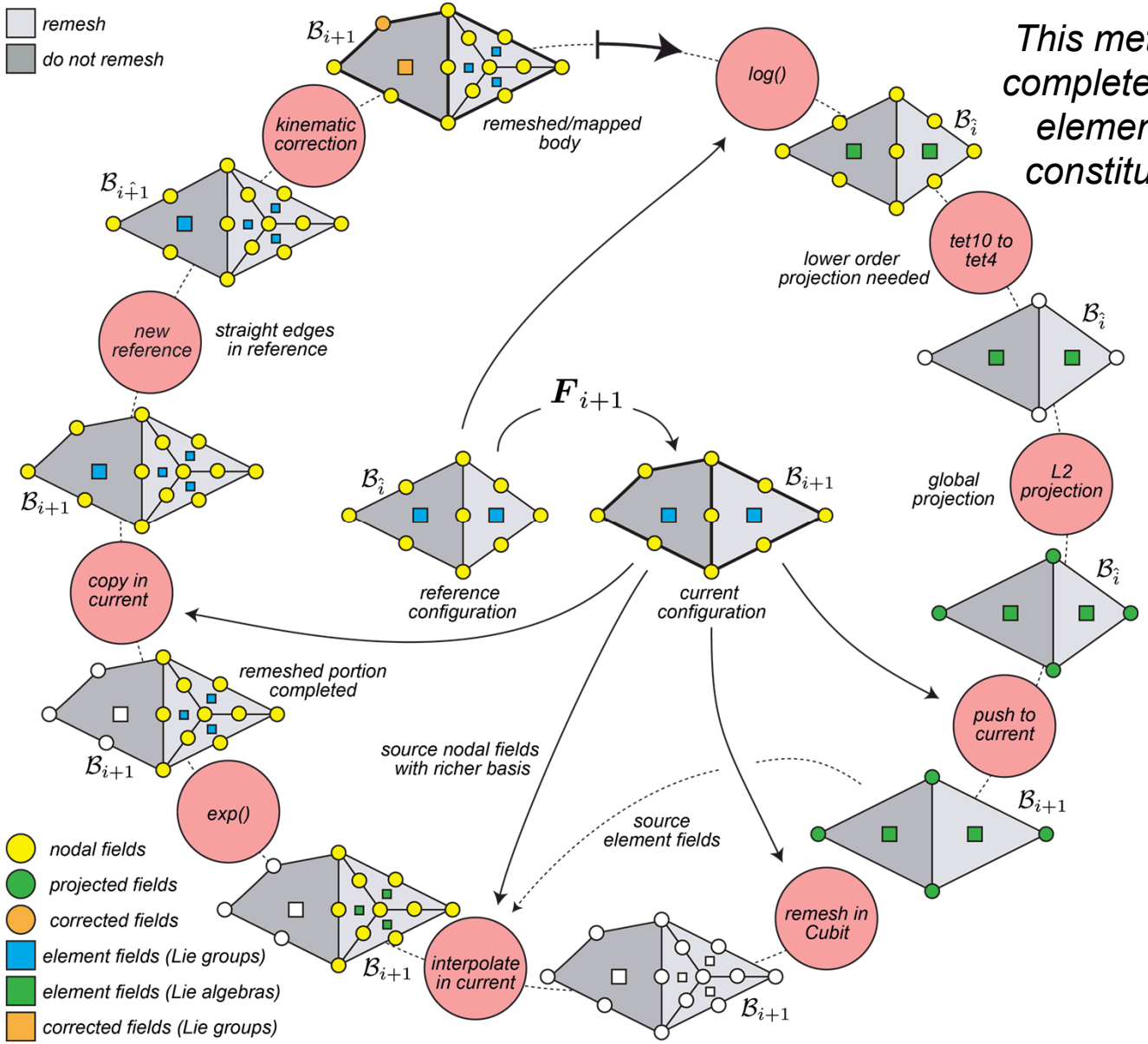

This methodology is completely general to element type and constitutive model.

Can we now model the loss of load-bearing capacity? Yes

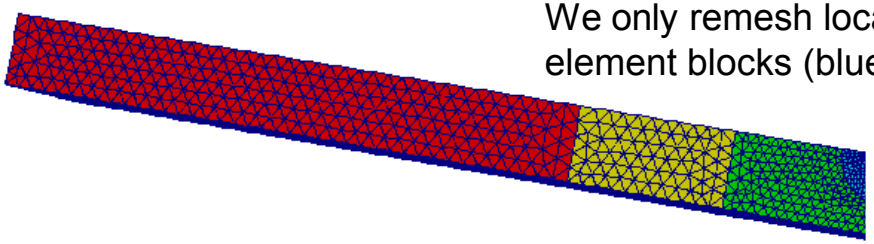

We only remesh local element blocks (blue)

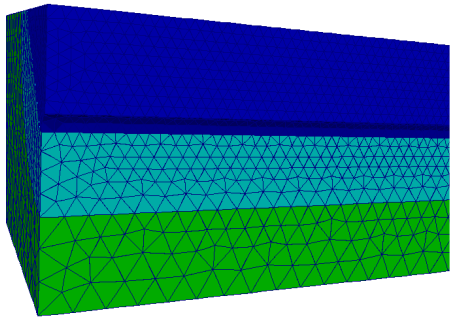

Composite-Tet10
Elements: 110,944
Nodes: 163,444
Yield stress: 196 MPa
Hardening: 2360 MPa
Recovery: 1.3

$$\sigma_y = Y + \kappa \qquad \dot{\kappa} = [H - R\kappa]\,\dot{\epsilon}_p$$

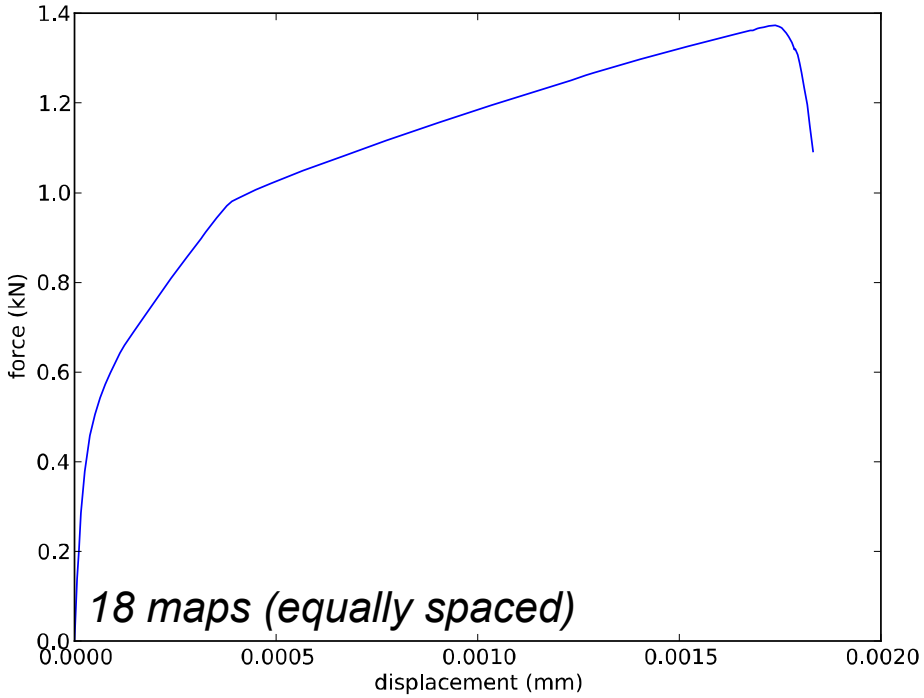

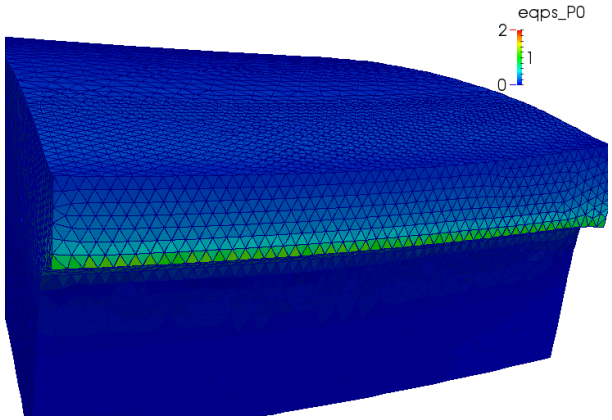

12th map

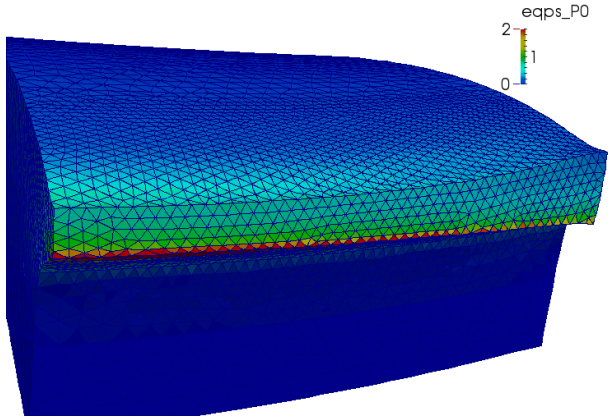

17th map

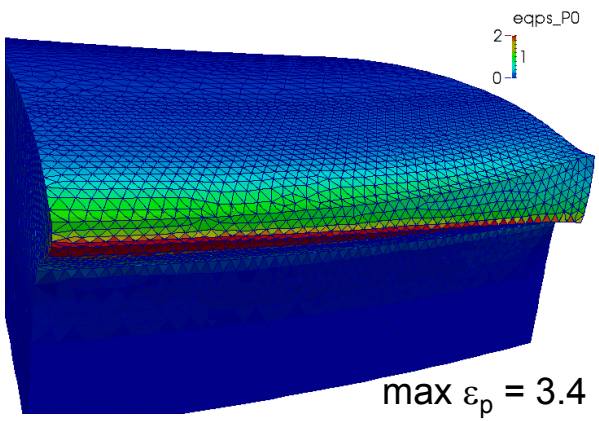

max ε_p = 3.4

18th map

Additional interior and exterior views of necking

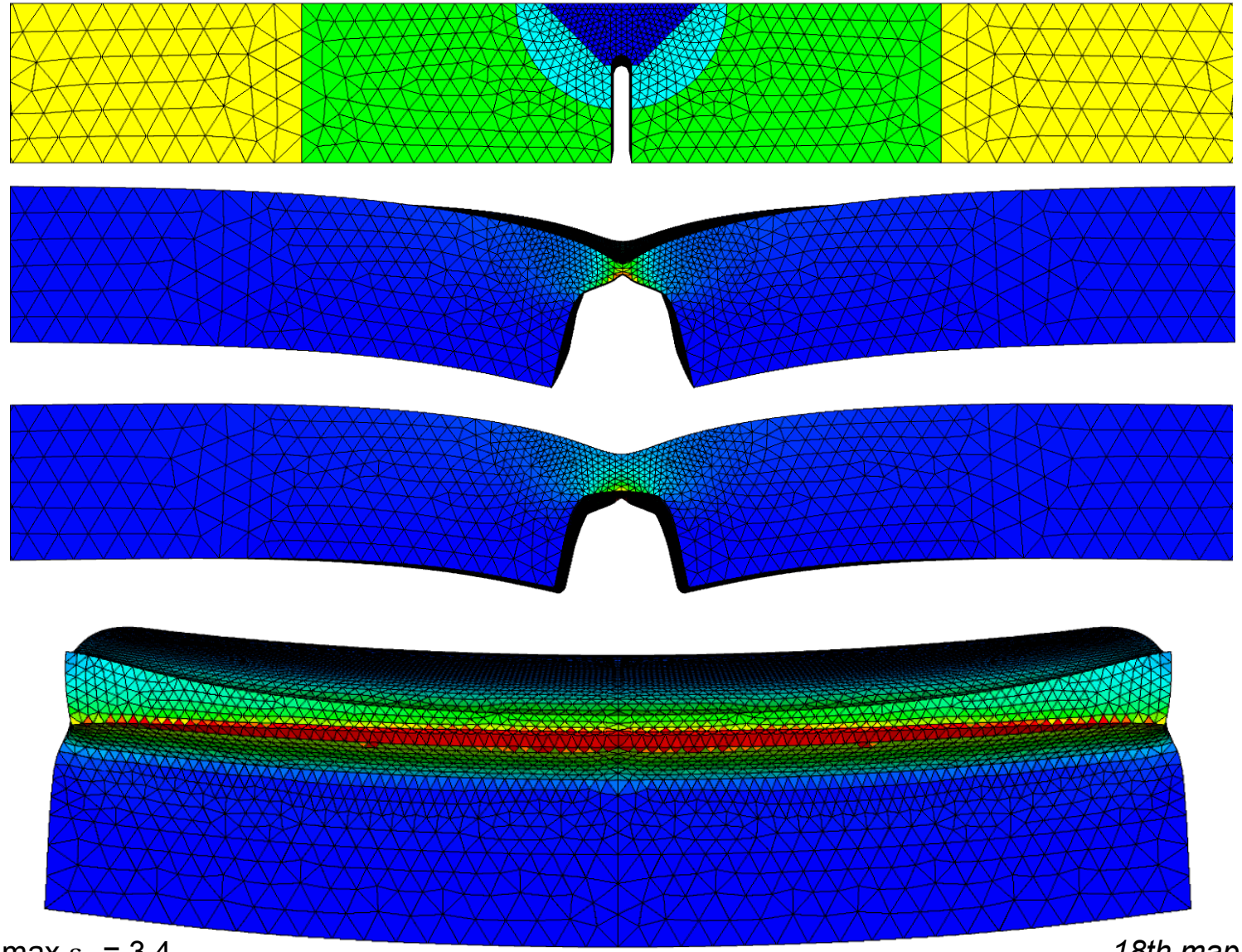

max ε_p = 3.4

18th map

Progress in modeling the evolution of pore structures

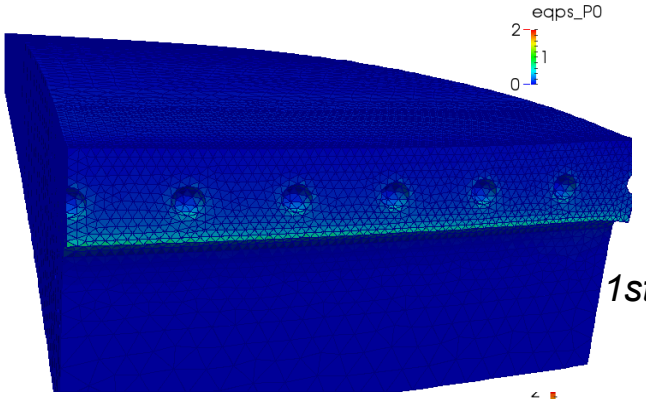

1st map

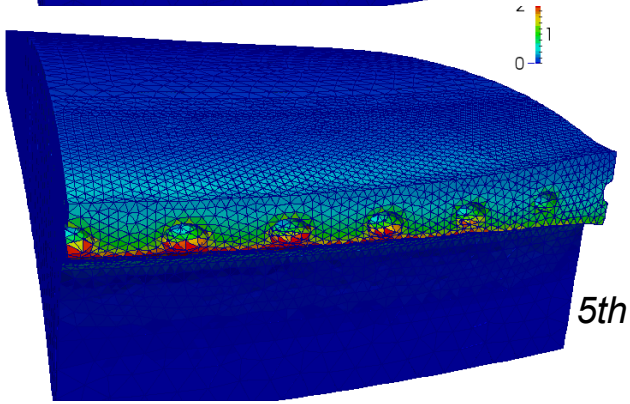

5th map

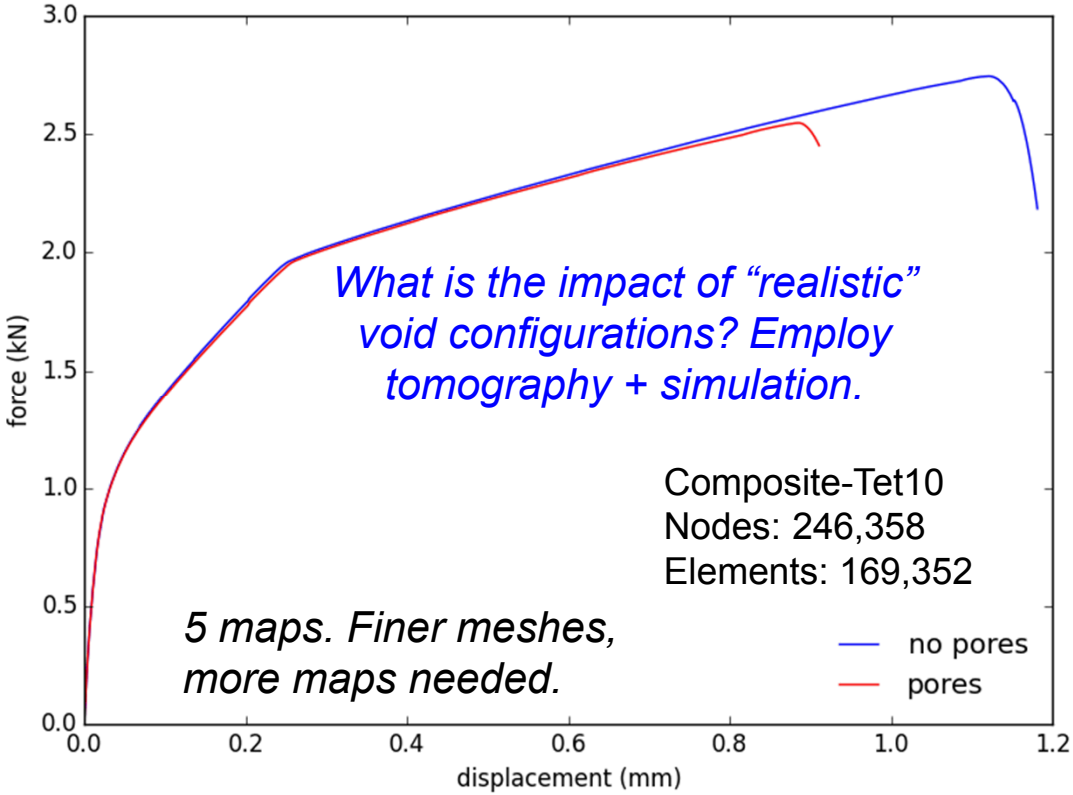

What is the impact of "realistic" void configurations? Employ tomography + simulation.

Composite-Tet10
Nodes: 246,358
Elements: 169,352

5 maps. Finer meshes, more maps needed.

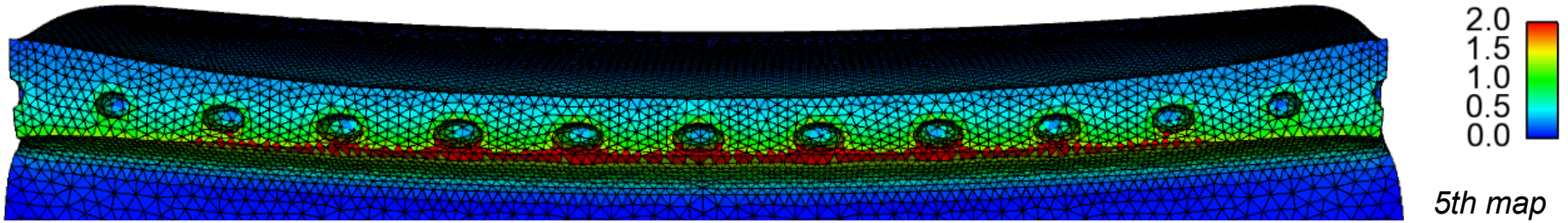

5th map

Additional interior and exterior views of necking w/pores

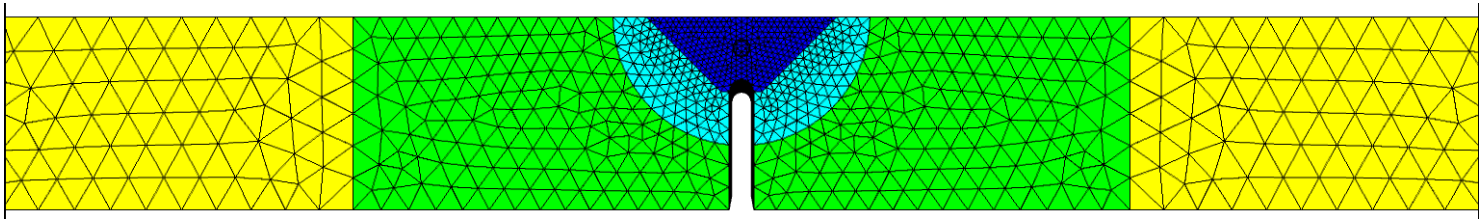

undeformed mesh with notch

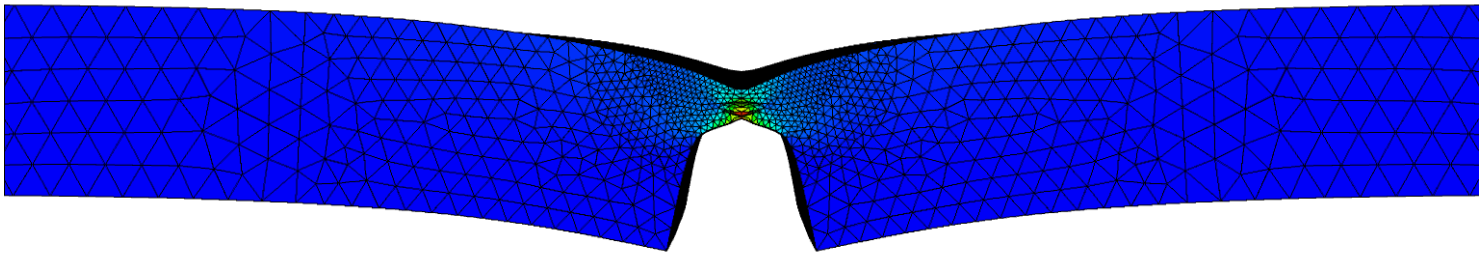

necking at mid-plane

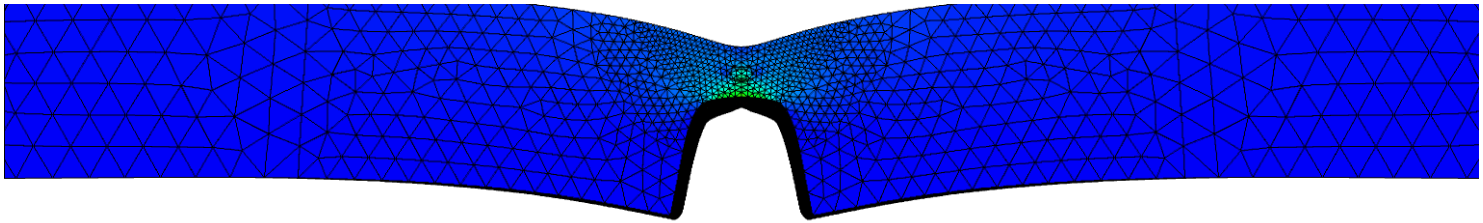

necking at surface

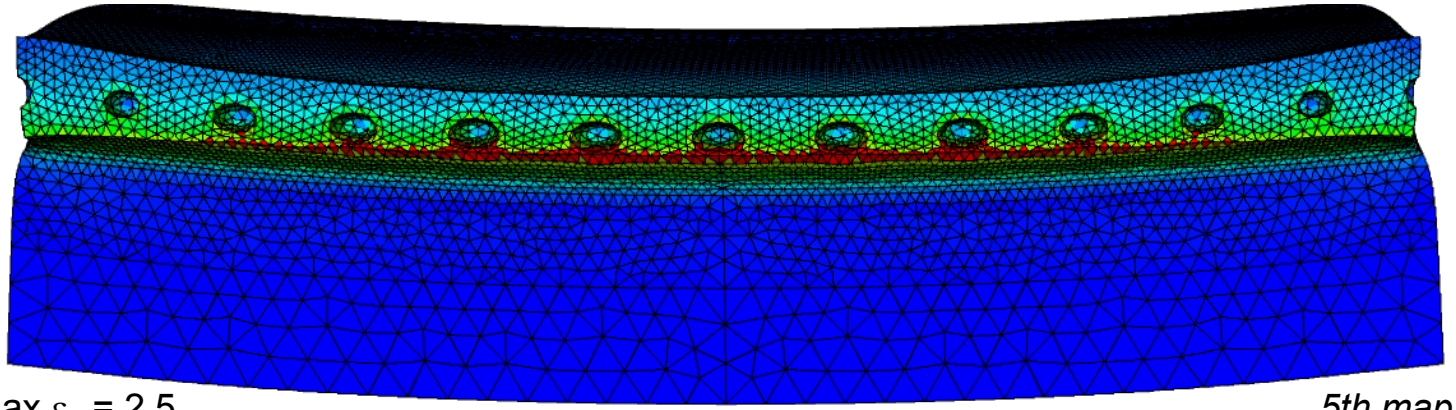

max ε_p = 2.5

5th map

Increasing the number of mappings

Sandia National Laboratories

Animation illustrating the deformation process with 31 maps

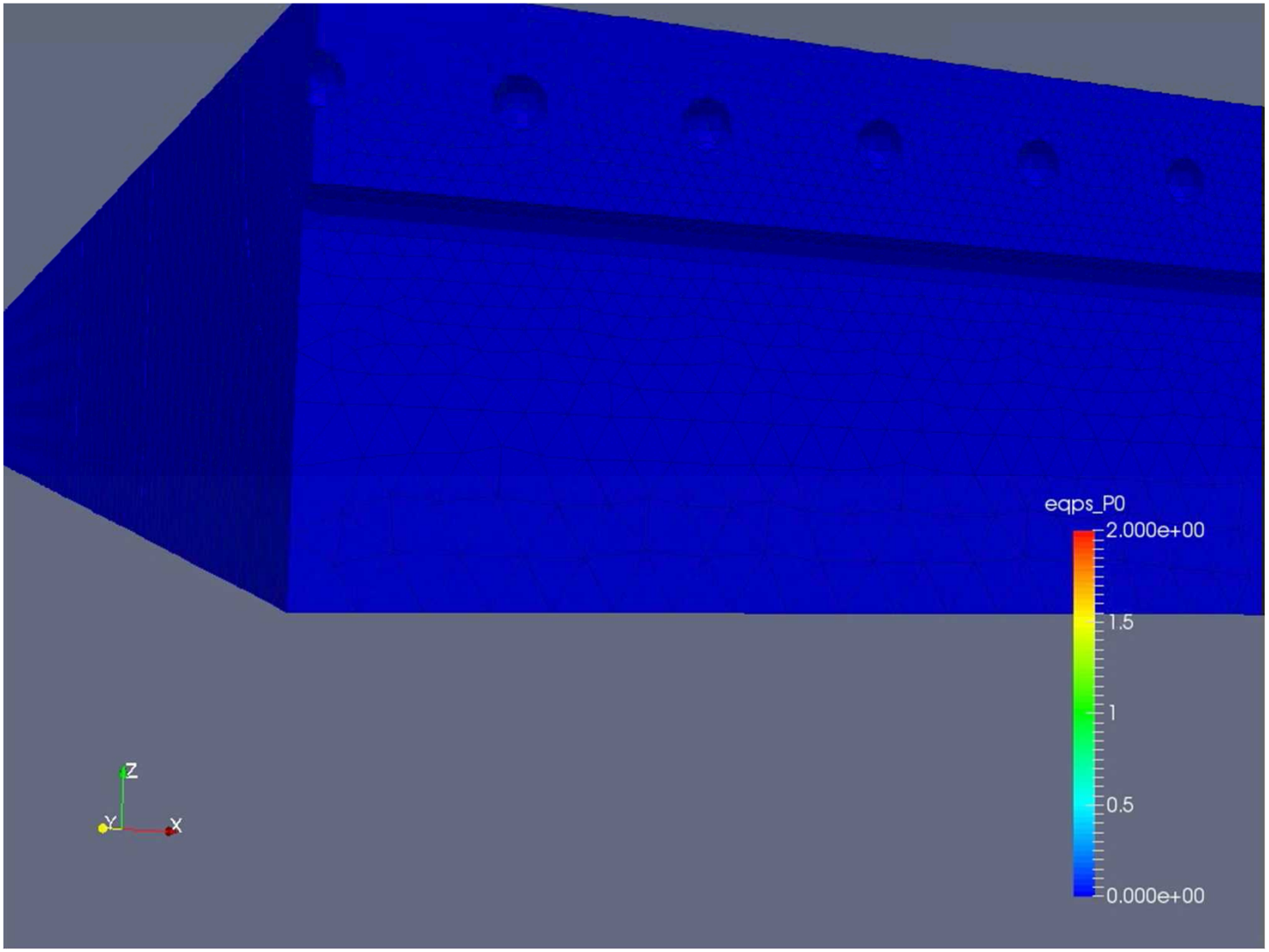

Conclusions and Path forward

- *mapLL* ensures a sound theoretical basis
- Tetrahedral elements permit discretization*
- Composite-tetrahedral elements resolve ISVs
- New reference configuration enables solution
- We are able to predict the load-bearing capacity
- General methodology for modeling localization

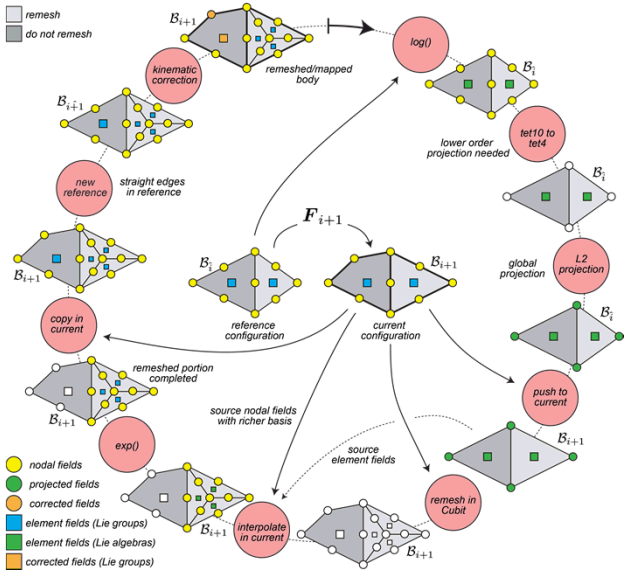

Path forward

- Increase robustness of remeshing
  - Mesh geometry in Cubit problematic
- Re-examine convergence
  - Mesh refinement
  - # maps / # intervals
- Model idealized void configurations

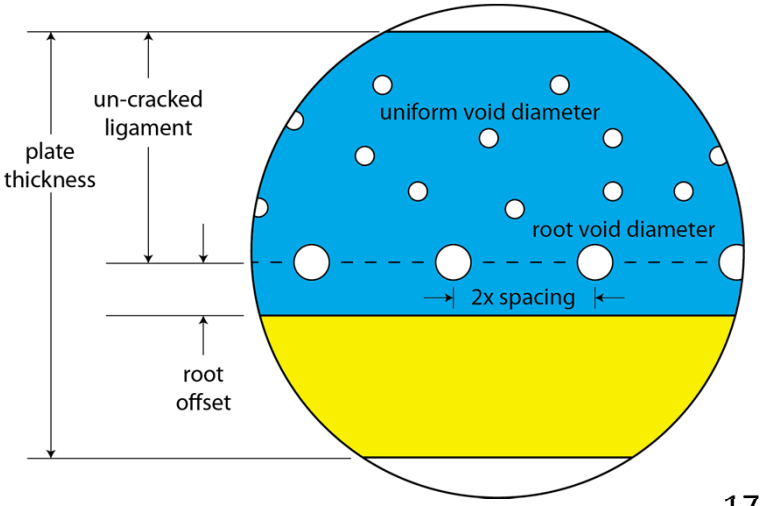

Adopting a new reference configuration

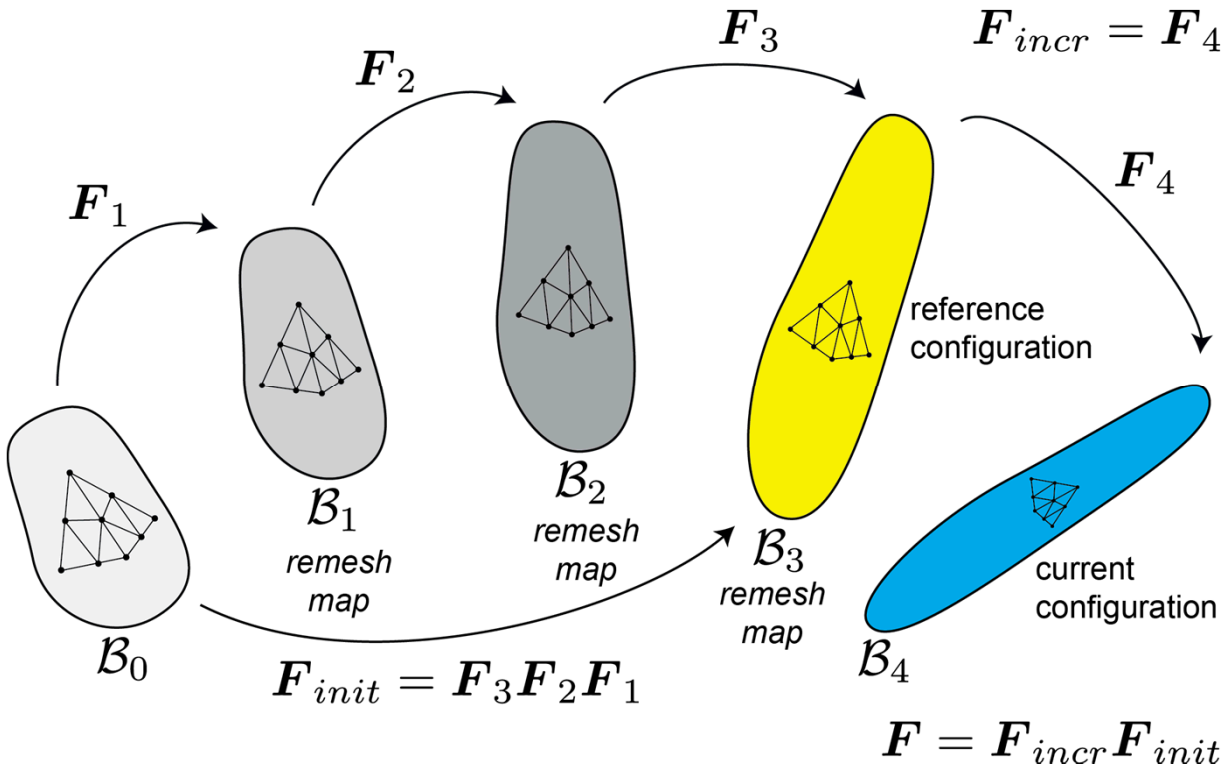

- Prior work on hexahedral elements maintained the reference configuration
- Elements degrade in the reference configuration - T-L element integrate in reference
- We now adopt a new reference configuration and map $\mathbf{F}_{init}$ (which lives in a Lie Group)